Calculated optical properties of thorium, protactinium, and uranium metals

T. Gasche*
Condensed Matter Theory Group, Department of Physics, Uppsala University, S-751 21, Sweden

M. S. S. Brooks
European Commission, Joint Research Centre, Institute for Transuranium Elements, Postfach 2340 D-76125 Karlsruhe, Germany

B. Johansson
Condensed Matter Theory Group, Department of Physics, Uppsala University, S-751 21, Sweden
(Received 26 September 1995; revised manuscript received 12 March 1996)

We report self-consistent energy band calculations using the linear muffin-tin orbital method and the local-spin-density approximation to exchange and correlation in density-functional theory for the light actinide metals Th, Pa, and U. The optical properties have been calculated and compared with measurements, where possible. The dependence of the optical response functions upon crystal structure was found to be surprisingly large and the dependence upon spin-orbit coupling, less so. Where it was possible to make comparison, agreement with experiment was obtained for the maxima of the optical spectra, the exception being a feature in the optical conductivity at 10 eV measured in both Th and U but not obtained in the calculations. [S0163-1829(96)02528-3]

I. INTRODUCTION

Self-consistent energy-band calculations for the ground states of the actinide metals, both scalar relativistic[1] and fully relativistic,[2] yield approximate agreement with experiment for the lattice constants of the elemental metals. More recently, full potential calculations have been used to calculate the total energies of different lattice structures as a function of volume[3] and, again, good agreement with experiment has been obtained.

One of the fundamental questions concerning the actinides is whether their f states are localized or itinerant and from this point of view it is of interest to compare theory and experiment for spectroscopic as well as ground-state properties. Optical spectroscopy, like photoelectron spectroscopy and bremsstrahlung isochromat spectroscopy, is a method which allows one to probe the states (both occupied and vacant) around the Fermi energy.[4,5] The effects of electron-electron correlation arising from $5f$ electron localization upon excited-state properties are stronger than upon ground-state properties as, for example, when the on-site attraction of electron and hole quasiparticles is strong. The most thorough spectroscopic studies of the light actinide metals are for thorium,[6–9] although there is less than satisfactory agreement between the different experiments.[8] Data are also available for uranium metal[10] but not for protactinium.

A comparison between early energy-band calculations[11,12] and the measured optical conductivity was used to argue that the Th $5f$ states are itinerant,[6] although no optical response functions had been calculated. Subsequently Fäldt and Nilsson[9] attempted to compare their measured spectra for Th,[9,10] with an optical response estimated from the energy band calculations of Skriver and Jan.[13] These early theoretical analyses[9,10] left many questions unanswered.[5] More recently, a theoretical study[14] of the optical properties of thorium metal explained quite well the measured structures in the dielectric function and optical conductivity. The only available calculations for uranium metal[10] estimated the optical response from energy-band calculations for the fcc structure,[1] although uranium at ambient pressure is orthorhombic. The aim of this paper is to compare the early actinides Th, Pa, and U, paying attention to both the role of their crystal structure and relativistic effects, and to give a thorough theoretical interpretation of the experimental data.

II. CALCULATION

We have calculated the band structure of Th, Pa, and U at their equilibrium lattice constants, both in the fcc structure and their actual structure types (Pa is tetragonal and U orthorhombic). This we have done within the linear muffin-tin orbital method,[15] using the von Barth and Hedin[16] exchange-correlation term in the local-spin-density approximation.[17]

The conductivity tensor is obtained from the Kubo formula[18,19]

$$\sigma_{ij}(\mathbf{q},w)=\left[\frac{iNe^2}{m\omega}\right]+\frac{1}{\hbar\omega}\int_{-\infty}^{0}dt \times\langle[j_i(\mathbf{q},0),j_j(-\mathbf{q},t)]\rangle\exp^{-i\omega t}, \quad (1)$$

and, for optical properties, the $q=0$ limit is appropriate. Then the conductivity and dielectric tensors are related by

$$\varepsilon_{ij}(w)=\delta_{ij}+\left[\frac{4\pi i\sigma_{ij}(0,w)}{\omega}\right]. \quad (2)$$

When Eq. (1) is evaluated over the set of single-particle energy-band states, the diagonal elements of the *interband* conductivity tensor become

$$\sigma_{ii}(\omega)=\frac{ie^2}{m^2\hbar}\sum_{\mathbf{k}}\sum_{l}\sum_{n}\frac{1}{\omega_{nl}(\mathbf{k})}\left[\frac{|\pi^i_{nl}(\mathbf{k})|^2}{\omega-\omega_{nl}(\mathbf{k})+i\delta}+\frac{|\pi^i_{nl}(\mathbf{k})|^2}{\omega+\omega_{nl}(\mathbf{k})+i\delta}\right][f_l(\mathbf{k})-f_n(\mathbf{k})], \quad (3)$$

where $f_n(\mathbf{k})$ is the Fermi distribution function, and l and n label initial and final energy-band states. Here the energies of transitions between energy-band states are $\omega_{nl}(\mathbf{k}) = \omega_n(\mathbf{k}) - \omega_l(\mathbf{k})$, and $\pi^i_{ln}(\mathbf{k})$ is a matrix element of the proper momentum operator between the branches n and l at the wave vector $\mathbf{k}$. In practice, the proper momentum operator π,

$$\pi = \mathbf{p} + \frac{\hbar}{4mc^2}[\sigma \times \nabla V(r)], \tag{4}$$

is replaced by $\mathbf{p}$ since the difference is small.

The matrix elements of the momentum operator between energy-band states expanded in an l,s basis set with the spherical symmetry of the atomic-sphere approximation[15]

$$|n\mathbf{k}\rangle = \sum_{lm} (i)^l C^{n\mathbf{k}}_{lm} \Phi_l(r) Y^m_l(\hat{\mathbf{r}}) \tag{5}$$

are

$$\langle n\mathbf{k}|\mathbf{p}|n'\mathbf{k}\rangle = \sum_{l,m_l,l',m_{l'}} (C^{n\mathbf{k}}_{lm_l})^* C^{n'\mathbf{k}}_{l'm'_l} \langle \Phi_l(r) Y^m_l |\mathbf{p}| \Phi_{l'}(r) Y^{m'}_{l'} \rangle, \tag{6}$$

and factor to a product of a radial component and an angular component.[20] The angular component is evaluated from the Wigner-Eckart theorem, leading directly to the optical selection rules $\Delta l = \pm 1$ and $\Delta m_l = \pm 1$. The radial component is evaluated by direct differentiation of the radial wave functions followed by integration. In cubic systems it is necessary to calculate only one of the three diagonal components of the dielectric tensor; however, some of the structures of Pa and U are not cubic, and we have calculated the sum of the diagonal elements of the conductivity and dielectric tensors.

In the present paper the imaginary part of the dielectric function was obtained by summation over the Brillouin zone. The real part was subsequently obtained by Kramers-Kronig transformation. These calculations yield the unbroadened functions. To reproduce the experimental conditions correctly, it is necessary to broaden the calculated spectra. The exact form of the broadening function is unknown, although comparison with measurements suggests that the broadening usually increases with increasing excitation energy.

The intraband contribution is approximated by

$$\varepsilon^{\text{intra}}(\omega) = 1 - \frac{\omega_p^2}{\omega(\omega + i\gamma)}, \tag{7}$$

where the free-electron plasma frequency is given by the Drude relationship $\omega_p^2 = 4\pi n e^2/m^*$, and γ is the relaxation frequency. The only available data for the intraband contribution are given by Weaver and Olson[7] for Th, who give $\sigma_{\text{dc}} = 1.79$ Ry and $\gamma = 0.0073$ Ry. In practice we find that the intraband contribution is negligible compared with the interband contribution above 0.5 eV, as is generally the case for metals with strong interband transitions.

The first calculations were scalar relativistic, where the spin-orbit interaction is set to zero, but the mass velocity and Darwin shifts are included properly. However, for uranium, the spin-orbit interaction parameter ζ for the $5f$ states is 0.2 eV, leading to a splitting between the $j = 3 \pm \frac{1}{2}$ bands of $\frac{7}{2}\zeta \approx 0.7$ eV, compared to a bandwidth of about 3 eV. Although uranium is nonmagnetic, the spin-orbit interaction in principle has an effect upon the electronic structure and chemical bonding. When the spin-orbit interaction is large it can split the 14 degenerate $5f$ bands into sets of $j = \frac{5}{2}$ and $\frac{7}{2}$ states with degeneracies of 6 and 8, respectively.[2] The $j = \frac{5}{2}$ states in a light actinide are therefore filled preferentially to the $j = \frac{7}{2}$ states. The resulting changes in cohesive properties arise from the fact that the antibonding orbitals of the $j = \frac{5}{2}$ bands are filled earlier than they would be if the spin-orbit interaction were zero and the $5f$ levels 14-fold degenerate. The actual magnitude of such effects can only be obtained from a complete self-consistent energy-band calculation, since the spin-orbit Hamiltonian is off-diagonal in an ls representation. Calculations[2] showed that the spin-orbit interaction starts to have an appreciable effect upon ground-state properties for Np and Pu since it is for these elements that the antibonding $j = \frac{5}{2}$ states are nearly filled. For Th-U the hybridization between the $j = \frac{5}{2}$ and $\frac{7}{2}$ states is large compared with the spin-orbit interaction, and cohesion is not altered significantly. The spin-orbit interaction does, however, increase the total $5f$ bandwidth, as may be seen from the following argument.[21] The width W of the $5f$ bands is essentially given by the second moment which is $W^2/12 = \text{Tr}(H^2)/14$, for a rectangular state density, where the trace runs over the $5f$ states and H is the Hamiltonian. If the width of the $5f$ bands in the absence of spin-orbit coupling is W_0, it easy to show that it is given by $W^2 = W_0^2 + 12\,\text{Tr}(\zeta \mathbf{l}\cdot\mathbf{s})^2/14$ in the presence of spin-orbit interaction. A little algebra shows that W^2 is increased by $36\zeta^2$. Since $\zeta \approx 0.2$ eV the change in the square of the width of the $5f$ states is about 1.5 eV, leading to an estimated increase in $5f$ bandwidth of about 0.25 eV for $5f$ bands with an original width of 3 eV. In practice for uranium metal, but not for Pu, the calculated state densities are very similar whether or not spin-orbit interaction is included. The same is true for the optical spectra. For Pa and Th these differences are even smaller. This may be seen in Fig. 1, where we compare the low-energy dielectric function for uranium with and without spin-orbit interaction. As the spin-orbit coupling splits the degenerate bands, it leads to a broadening of the optical spectra; thus the peaks for the case with spin-orbit coupling tend to be broader but lower than the respective peaks calculated without spin-orbit coupling.

III. ANALYSIS

Prior to making any comparisons between theory and experiment, we wish to make some general comments about the expected accuracy of our calculations. As stated in Sec. II, we expect the eigenvalues, and thus the transition energies, to be more accurate than the magnitude of the conductivity which involves transition matrix elements, provided that single-electron theory is a good approximation. We have therefore analyzed the energies of transitions in detail.

As most experimental data are available for Th, we shall begin our analysis with Th (Fig. 2). Above 4 eV, the various measurements of the conductivity vary by a factor of 2 in

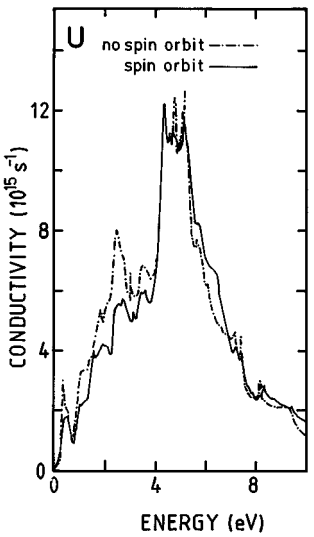

FIG. 1. Calculated optical conductivity for uranium with and without spin-orbit interactions.

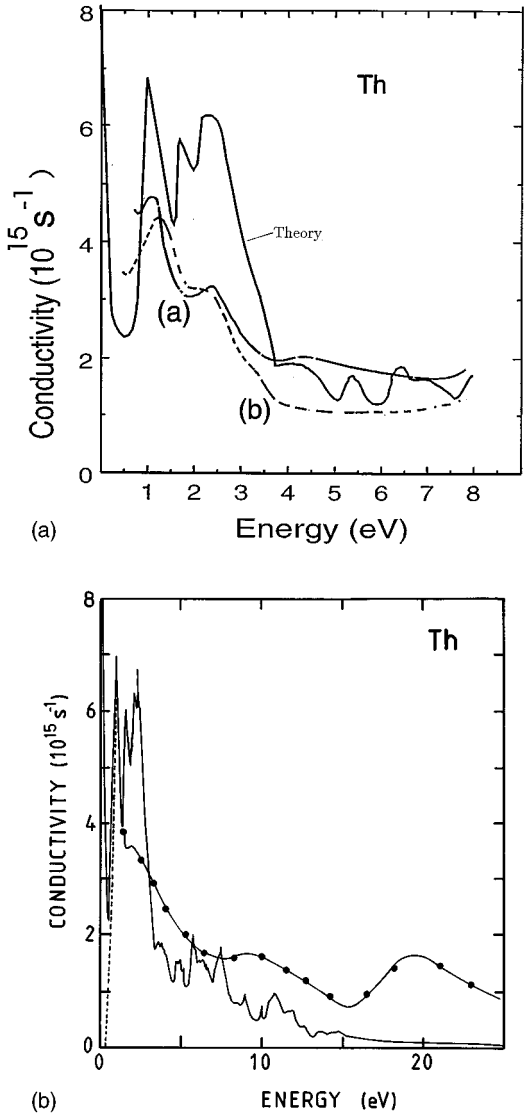

FIG. 2. Conductivity of thorium. (a) Low-energy range: experimental, [(a) Fäldt and Nilsson (Ref. 9) and (b) Alvani and Naegele (Ref. 8)]. Note that the data of Weaver and Olsson (Ref. 7) are very similar to that of Alvani and Naegele], and theoretical. (b) Full energy range: experimental [(Ref. 9) (full line with points)] and theoretical (unsmoothed) conductivities. Both figures include a Drude contribution, as given by Eq. (7).

magnitude. This may well be because, as discussed in Refs. 8 and 9, the samples are known to have a considerable dependence on surface preparation. In Fig. 2(a), apart from the available experimental data, we also show the calculated conductivity for Th. The first maximum is clearly seen: for the second experimental maximum we have two maxima. Application of a broadening function results in these two maxima combining to form the second maximum at 2 eV; theoretical and experimental maxima are presented in Table I. At higher energies [see Fig. 2(b)] the general decrease is reproduced (note that we have not smoothed the high-energy curve), but there are two shortcomings. The first is the experimental feature at 9 eV, the second is the broader feature at 19 eV. Considering the density of states, it is impossible to find features that could correspond to this broad 19-eV feature. As discussed in Ref. 9, x-ray photoemission places the Th $6p_{3/2}$ states 16.8 eV below the Fermi energy.[22,23] We have made two self-consistent calculations for free atoms to check this feature at 19 eV. First, for a normal Th atom we found that the $6p_{3/2}$ states lie about 20 eV below the center of the $6d_{3/2}$ and $6d_{5/2}$ states. Second, we made a transition-state calculation,[24] by taking one-half of an electron out of the $6p_{3/2}$ core state and placing in the $6d_{3/2}$ and $6d_{5/2}$ states, weighted according to their degeneracy—thus allowing for relaxation. In this case the $6p_{3/2}$ states lie 19.9 eV below the center of the $6d_{3/2}$ and $6d_{5/2}$ states. We therefore assign this 19-eV feature to $6p \rightarrow 6d$ transitions. The breadth is due to the width of the $6d$ band final states. In our calculations the $6p$ states are treated as core states, which are therefore not included in possible transitions.

We do not obtain the lower feature at 9 eV. However, since reflectivity is a bulk property, it is quite likely that actinide samples, which normally contain some oxygen, will somewhere produce a feature from the oxygen. In the optical spectrum for ThO_2 or UO_2,[23,25,26] the dielectric function $\varepsilon_2(\omega)$ contains features at 8–11 eV, and we suspect that these same features appear in the metal.

We now consider the low-energy range. We calculate two peaks, at the same energy as seen in the experiments. The origin of the low-energy features is normally analyzed through the joint state density. The joint state density is evaluated with Eq. (1), setting the matrix elements in Eq. (2) equal to a constant. This is equivalent to ignoring the selection rules and the variation of the radial integral over the different wave functions. The joint state density is shown in Fig. 3. By looking at the state density, Fig. 3, the rise in the joint state density between 2 and 3 eV is seen to come from transitions from feature 2 to feature 3, while the feature at 5 eV comes from 1-3 and 2-4 transitions. This is in good agreement with the work of Skriver and Jan.[13] As pointed out by Fäldt and Nilsson, one would expect the conductivity to have the appearance of the joint state density as the joint state density arises (primarily) from transitions from the d states to the empty f bands, and thus does not contravene the optical selection rules ($\Delta l = \pm 1, \Delta m_l = \pm 1$). If this were re-

TABLE I. Summary of theoretical and experimental features.

	Th		*U*	
Feature	experiment[a]	theory	experiment[b]	theory
A	1.2	1.1	0.7	0.3
B	2.3	2.0	1.4	1.5
C			3.8	5.0
oxide feature	9.0	8.5–10.5[c]	10.0	7.5–10.0[c]
$6p \rightarrow 6d$	19.0	18.8[d]	19.0	19.0[d]

[a]Fäldt and Nilsson (Ref. 9).
[b]Fält and Nilsson (Ref. 10).
[c]From calculations for ThO_2 and UO_2 (Ref. 26).
[d]Estimated from the x-ray photoemission initial state (Ref. 23) and band final state.

ally the case, then a large feature at 5 eV should appear in the conductivity. By considering individual transitions, we find that the situation is more complicated than it first appears. While $d \rightarrow f$ transitions are allowed, the oscillator strength is found to be nearly zero, as shown in Table II. The feature at 1.1 eV arises from $p,f \rightarrow d$ transitions as the lower-f feature in Fig. 3 has a non-negligible d occupation. The f,p occupation of feature 1 and the d occupation of feature 4 in the state density are much lower, and so there are no noticeable transitions for this 5-eV energy range. Thus, although the 2-eV feature arises from transitions into $5f$-derived bands,[9] the transitions are actually to the d admixture of these states. It is the absence of d admixture in the higher $5f$ bands that leads to the absence of any significant 5-eV feature.

Since we have found that the strength of $d \rightarrow f$ transitions is much less than that of $f \rightarrow d$ transitions, which, to our knowledge, is the first time that such a claim has been made, some explanation is required—particularly in view of the fact that the momentum operator is Hermitian. For any given energy the matrix elements for $d-f$ and $f-d$ transitions are equal. However, in the actinides both occupied and excited $6d$ states in the energy range of interest are at the bottom (the bonding part) of the $6d$ bands, which are over 1 Ry broad. There is therefore little energy dependence in the $6d$ wave functions, which are essentially bonding bands up to energies greater than 7 eV. In contrast, the $5f$ bands are narrow, their width being only a few eV. The occupied part of the $5f$ bands are bonding, whereas the unoccupied $5f$ bands at energies of more than 3 eV above the Fermi energy are antibonding. We have illustrated the situation by plotting the wave functions in Fig. 4. Transitions from occupied $5f$ states to unoccupied $6d$ states are from bonding to bonding bands, and over most of the atom the derivative operator in the momentum matrix element operates on a wave function with negative slope. In contrast, transitions from occupied $6d$ states to unoccupied $5f$ states are from bonding to antibonding bands, where the slope of the wave function changes sign, leading to cancellation and small transition matrix elements. Thus, although the matrix elements of the momentum operator are Hermitian, asymmetry in the nature of the energy dependence of the $5f$ and $6d$ states, and the fact the antibonding $5f$ states lie only a few eV above the Fermi energy, lead to asymmetry in the oscillator strengths of $f \rightarrow d$ and $d \rightarrow f$ transitions. There has been discussion in the literature concerning the large feature observed at 4 eV by Veal, Koelling, and Freeman.[6] Weaver and Olsson[7] claim that this is correlated with surface roughness (a surface plasmon), and while we cannot confirm this we find no such

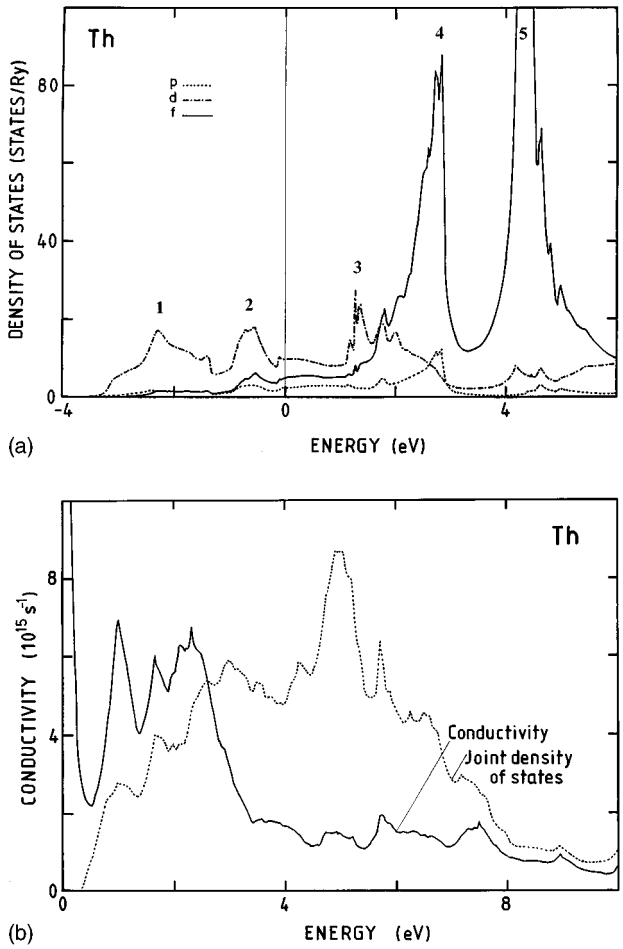

FIG. 3. Thorium fcc: (a) State density (with features as referred to in Table II). (b) Joint density of states and conductivity.

TABLE II. Calculated oscillator strength $|\langle \phi_f | \nabla | \phi_i \rangle|^2$ for Th for transitions between the features marked in Fig. 3. The letters in the first column refer to l quantum number of the initial and final states.

	1→3	1→4	1→5	2→3	2→4	2→5
Energy (eV)	3.5	4.5	6.5	2.0	3.0	5.0
$f \rightarrow d$	0.314	0.302	0.270	0.221	0.212	0.185
$p \rightarrow d$	0.518	0.533	0.593	0.476	0.490	0.548
$d \rightarrow p$	0.012	0.010	0.006	0.039	0.003	0.002
$d \rightarrow f$	0.002	0.001	0.022	0.004	0.000	0.002

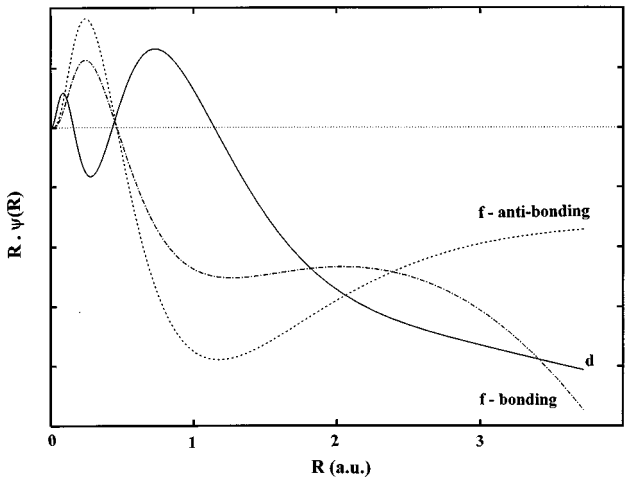

FIG. 4. Calculated thorium d and f wave functions. The f-wave functions are calculated at -2.0 eV (bonding) and 2.5 eV (antibonding). The d-wave function shows very little variation over this interval.

appreciable structure in our bulk optical spectrum.

There are no data for Pa, but one would expect the same features at high energy as for Th. There is no great difference between the state density for bct, bcc, and fcc at equilibrium volume, as shown in Fig. 5 (it should be remembered that both Pa bct and fcc are arrived at from the bcc structure by a distortion in the z axis, so these structures are similar). All three densities are dominated by f states, forming two main peak systems. The first lies at between 1 and 2 eV, the second at 3 eV. At first glance the d states appear less important, but the partial d-state densities differ from one structure to another. The calculated conductivity is shown in Fig. 6, where for the fcc structure it has two noticeable features, at 2 and 4 eV, in contrast to the bcc and bct structures, which are relatively flat. The explanation for this is the same as for Th: the $d \rightarrow p,f$ oscillator strength is extremely low, and the optical spectra results from $f \rightarrow d$ transitions. Looking at the partial state densities, Fig. 5, we immediately see the feature in the d-state density for fcc at 1 eV. It is this final state that gives rise to the two features. Other than this, the conductivities are relatively featureless due to the flatness of the d-state density above the Fermi energy.

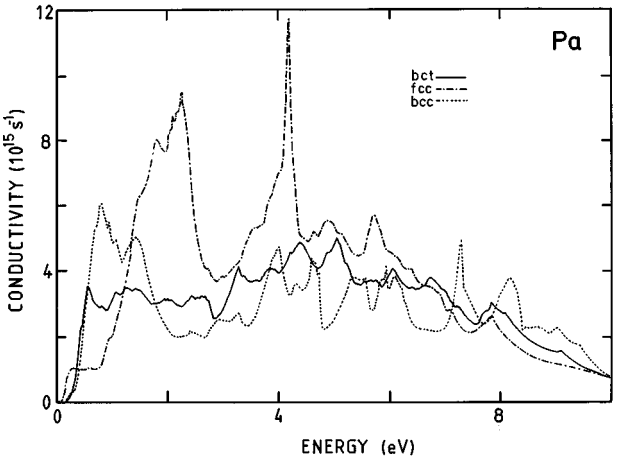

FIG. 6. Theoretical protactinium conductivity.

Unlike Pa, the state density for fcc U is noticeably different from that of its ground-state crystal structure (α-U), Fig. 7. As for Th and Pa, the $d \rightarrow p,f$ oscillator strength is extremely low, and it is the $f \rightarrow d$ transitions which dominate. As before, the fcc structure contains a feature in the unoccupied d state density, and this gives rise to two optical features, at 2.2 and 4.5 eV. The conductivity for α-U is much more smeared out; this is an immediate response to the al-

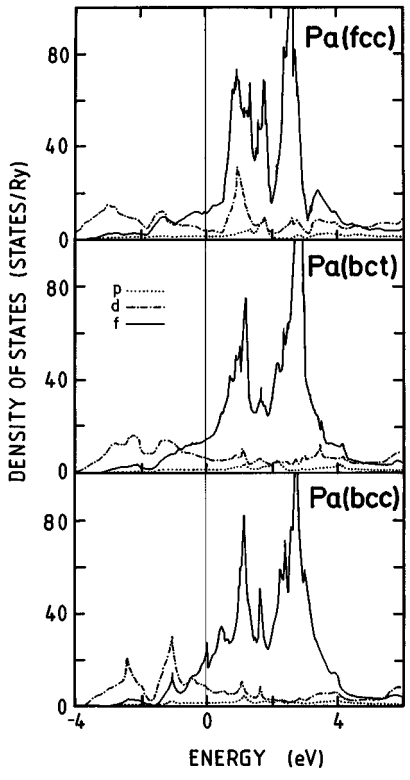

FIG. 5. Protactinium state density—fcc, bct, and bcc.

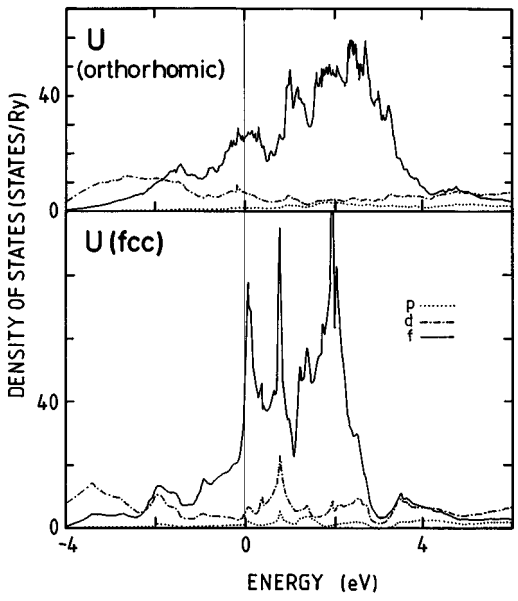

FIG. 7. Uranium state density—α-U and fcc.

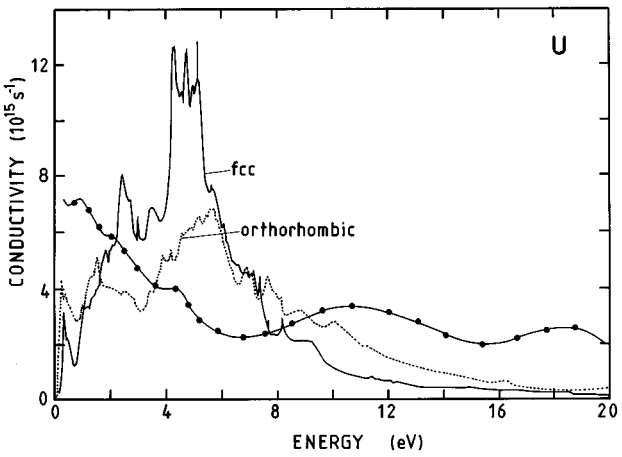

FIG. 8. Experimental (Ref. 10) (full line with points) and calculated optical conductivities of uranium metal.

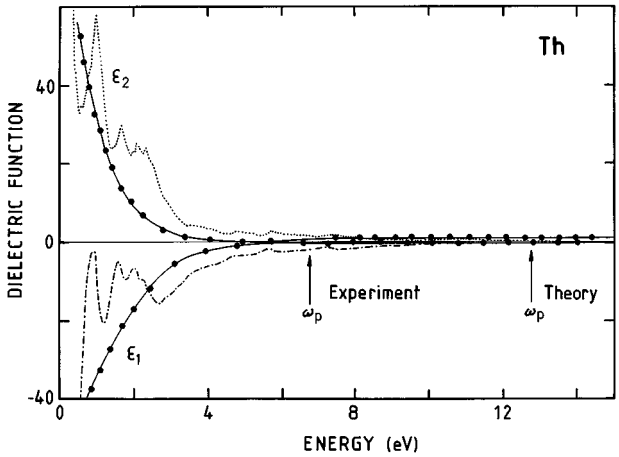

FIG. 9. Experimental (Ref. 9) (full line with points) and calculated real and imaginary parts of the dielectric function of thorium metal.

most constant d-state density above the Fermi energy (see Fig. 8). Over this background we see rises in intensity at 0.3, 1.5, and 5.0 eV. Applying a broadening of 0.3 eV (not shown here) simply has the effect of lumping together the minor peaks to produce the three rises noted above. Comparing this with experiment[10] we see features at 0.7, 1.4, and 3.8 eV, although the intensity seems too low for the first two features. This could be improved by the addition of a Drude term. As for the case of Th, there is poor agreement as regards the magnitudes of the peaks. The possible explanations for this are, as for Th, due to both experimental and theoretical considerations. As before, we assign the higher features, at 10 and 19 eV, to oxide and $6p \rightarrow 6d$ transitions,[10] respectively. Fäldt and Nilsson have attempted to compare the spectra for Th and U,[9,10] with the aid of bandstructure data (joint state density for Th provided by Skriver and Jan[13]). Unfortunately, their analysis is invalidated by the near-zero strength of the $d \rightarrow f$ transitions. They also compared the three features 1.2, 2.3, and 4 eV in Th with 0.7, 1.4, and 3.8 for U and, tentatively, stated that they where analogous. Given that the f bands fall by 3 eV from Th to U (from bremsstrahlung isochromat spectroscopy measurements[27]) the d band must then fall by more than 2 eV to maintain this feature distribution. This argument is refuted by our calculations, which find that the $d \rightarrow f$ oscillator strength is practically zero, and that for Th it is the d final state that plays the dominant role, whereas in U it is the U f initial state that dominates.

In Table I we summarize the theoretical and experimental features in these spectra. As commended upon above, there is generally good agreement for the energies of the theoretical and experimental features. Taking the $6p_{3/2}$ state as localized 17.3 and 18 eV below the Fermi energy for Th and U,[23] we then need a d state 1–2 eV above the Fermi energy to provide the final state. For Th this is clearly seen, but for U the possible d features are much smaller. This correlates very nicely with the experimental observation that the $6p \rightarrow 6d$ transition is weaker for U than for Th.

IV. ELECTRON-ENERGY-LOSS SPECTRA

The experimental electron-energy-loss spectra (EELS) for Th and U (Refs. 9 and 10) appear quite similar, rising gently from zero to a small feature at 7 eV, continuing to 13 eV (Th) and 15 eV (U), and then decreasing, both with a smaller feature at 20 eV. This similarity is hardly surprising due to the similarity in the conductivity. The low intensity of these three features is indicative of strongly damped plasma oscillations. The 7-eV feature comes from the passing of $\varepsilon_1(\omega)$ through zero, the higher features essentially from decreases in $\varepsilon_2(\omega)$. Theoretically this behavior is not reproduced. The calculated dielectric function for thorium metal is shown in Fig. 9. The resulting calculated energy-loss and surface energy-loss spectra, evaluated from $1/\varepsilon$ and $1/\varepsilon+1$, are shown in Fig. 10, together with the experimental electron-energy-loss spectra. We find that the electron plasma frequency $[\varepsilon_1(\omega)=0]$ is around 15 eV. This is approximately independent of (reasonable) values for Drude constants. This plasma frequency then gives rise to a massive feature at 15 eV, approximately a factor of 10 higher than the experimental feature. Furthermore, we have no feature of 7 eV in the calculated EELS but a small feature in the surface EELS at between 8 and 9 eV, in agreement with Eckardt.[14] The introduction of a feature at 10 eV in the conductivity has the

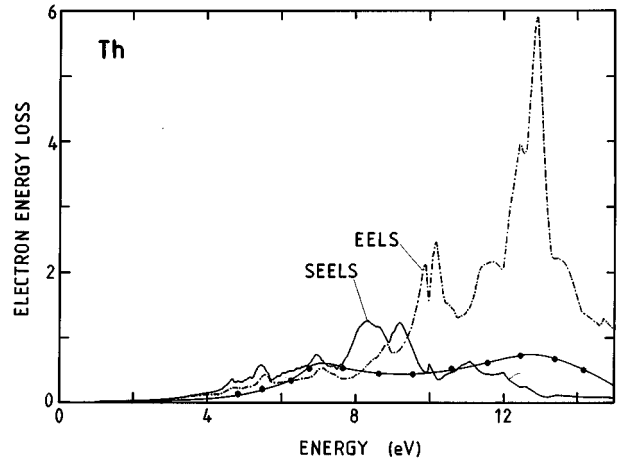

FIG. 10. Experimental (Ref. 9) (full line with points) and calculated electron energy loss and surface electron energy loss for thorium metal.

effect of damping the calculated EELS [as $\varepsilon_2(\omega)$ is thereby increased]. Thus, not only is the experimental intensity badly reproduced but the origin of the 13–15-eV features is different in theory and experiment. We suspect that the oxide acts to inhibit the largest EELS feature, which would, therefore, not be representative to pure Th or U. Whether these discrepancies arise solely due to theory or whether experimental difficulties play a role is, at present, hard to say; we know, however, that the only two high-energy spectra measurements were performed on samples with probable oxygen contamination, and on samples that are sensitive to surface treatment.

V. CONCLUSIONS

We have shown the spin-orbit interaction is not of major importance for the calculation of optical properties of uranium, but that the crystal structure has a surprisingly large effect. The state densities for bcc, bct, and fcc Pa are similar, yet the optical conductivities are noticeably different. This is a result of the near-zero $d \rightarrow f$ oscillator strength which means that the small differences in the distributions of d final states are important. It would therefore be interesting to measure the optical properties of these actinides under pressure. Either a change of crystal structure or a change in the $d \rightarrow f$ oscillator strength could result in a marked change of the optical properties.

These results imply that the $5f$ states in the early actinides are itinerant, which is hardly surprisingly given the great bulk of evidence for this conclusion.[28] This is similar to the conclusions of x-ray photoemission and bremsstrahlung isochromat spectroscopy.[27]

Lastly, the presence of oxygen in the early experiments is implied by the lack of any feature around 10 eV in the theoretical curves. It would be interesting to see additional experiments on Th and U (or, indeed, some data on Pa) if it were possible to produce them in an oxygen-free manner. Specifically, one could investigate our prediction of a drastic change in the EELS.

ACKNOWLEDGMENTS

T.G. would like to thank the Commission of the European Communities for a doctoral grant during which this work was initiated. T.G. and B.J. are also grateful to the Swedish Research Council for support.

*Present address: Departamento de Física, Universidade de Aveiro, Aveiro, Portugal.

[1] H. L. Skriver, O. K. Andersen, and B. Johansson, Phys. Rev. Lett. **41**, 42 (1978).
[2] M. S. S. Brooks, J. Phys. F **13**, 103 (1983).
[3] J. M. Wills and O. Eriksson, Phys. Rev. B **45**, 13 879 (1992).
[4] Y. Baer, in *Handbook on the Physics and Chemistry of the Actinides*, edited by A. Freeman and G. Lander (North-Holland, Amsterdam, 1984) Vol. 1, Chap. 4.
[5] See, e.g., the review by J. Schoenes, in *Handbook on the Physics and Chemistry of the Actinides* (Ref. 4), Vol. 1, Chap. 5.
[6] B. W. Veal, D. D. Koelling, and A. J. Freeman, Phys. Rev. Lett. **30**, 1061 (1974).
[7] J. H. Weaver and C. G. Olson, Phys. Rev. B **15**, 4602 (1977).
[8] C. Alvani and J. Naegele, J. Phys. Paris Colloq. **40**, C4-131 (1979).
[9] Å Fäldt and P. O. Nilsson, Phys. Rev. B **22**, 1740 (1980).
[10] Å Fäldt and P. O. Nilsson J. Phys. F **10**, 2573 (1980).
[11] R. P. Gupta and T. L. Loucks, Phys. Rev. B **3**, 1834 (1971).
[12] D. D. Koelling and A. J. Freeman, Solid State Commun. **9**, 1369 (1971).
[13] H. L. Skriver and J. P. Jan, Phys. Rev. B **21**, 1489 (1980).
[14] H. Eckardt, J. Phys. F **15**, 2451 (1985).
[15] O. K. Andersen, Phys. Rev. B **12**, 3060 (1975).
[16] U. von Barth and L. Hedin, J. Phys C **5**, 1629 (1972).
[17] W. Kohn and L. Sham, Phys. Rev. A **140**, 1133 (1965).
[18] R. Kubo, J. Phys. Soc. Jpn. **12**, 570 (1957).
[19] J. Callaway, *Quantum Theory of the Solid State* (Academic, New York, 1976).
[20] C. Koenig and K. A. Khan, J. Phys. C **27**, 6129 (1983).
[21] W. A. Harrison, Phys. Rev. B **28**, 550 (1983).
[22] J. Fuggle, A. Burr, W. Lang, L. Watson, and D. Fabian, J. Phys. F **4**, 335 (1974).
[23] B. W. Veal and D. J. Lam, Phys. Rev. B **10**, 4902 (1974).
[24] J. C. Slater, *The Self Consistent Field for Molecules and Solids; Quantum Theory of Molecules and Solids* (McGraw-Hill, New York, 1974), Vol. 4.
[25] J. Schoenes Phys. Rep. **63**, 301 (1980).
[26] T. Gasche and M. S. S. Brooks (unpublished).
[27] Y. Baer and J. K. Lang Phys. Rev. B **21**, 2060 (1980).
[28] M. S. S. Brooks, B. Johansson, and H. L. Skriver, in *Handbook on the Physics and Chemistry of the Actinides* (Ref. 4), Vol. 1, Chap. 3.